

Power-law distribution of pressure fluctuations in multiphase flow

S. Gheorghiu,* J. R. van Ommen, and M.-O. Coppens

Department of Chemical Technology, Delft University of Technology, Julianalaan 136, 2628 BL Delft, The Netherlands

(Received 25 November 2002; published 29 April 2003)

Bubbling fluidized beds are granular systems, in which a deep layer of particles is set in motion by a vertical gas stream, with the excess gas rising as bubbles through the bed. We show that pressure fluctuations in such a system have non-Gaussian statistics. The probability density function has a power-law drop-off and is very well represented by a Tsallis distribution. Its shape is explained through the folding of the Gaussian distribution of pressure fluctuations produced by a monodisperse set of bubbles, onto the actual distribution of bubble sizes in the bed, assuming that bubbles coalesce via a Smoluchowski-type aggregation process. Therefore, the Tsallis statistics arise as a result of bubble polydispersity, rather than system nonextensivity.

DOI: 10.1103/PhysRevE.67.041305

PACS number(s): 45.70.Mg, 47.55.Kf, 05.40.-a, 47.55.Dz

I. INTRODUCTION

Fluidized beds are a common form of a chemical reactor, in which a stream of gas is blowing upward through a deep layer of fine solid particles, setting it in motion. At a certain gas velocity, known as the minimum fluidization velocity U_{mf} , balance between gravity and drag is achieved, and the particles become suspended without being transported. Increasing the gas velocity above U_{mf} results in the excess gas flowing through the bed as bubbles. The mixture is said to be “fluidized,” and behaves in a way surprisingly similar to that of a bubbling liquid (see, e.g., Ref. [1] for a primer on fluidization). Despite this intuitive picture, the hydrodynamics of this two-phase system are highly complex and different from those of gas-liquid systems (e.g., there is no analog to surface tension, and the gas-solid interface is not well defined). The excellent mass and heat transfer properties of fluidized beds make them the solution of choice for applications such as combustion of solid fossil fuels and biomass, many exothermic reactions in the chemical industry, oil refinery, several metallurgical as well as biochemical and environmental cleanup processes. They are also extensively used to heat, cool, dry, or coat particles such as pharmaceuticals.

The present study uses a time series measurement of pressure to characterize the hydrodynamics. Pressure has significant advantages over other measurements in fluidization technology. Cornerstone techniques in flow research such as thin-film anemometry or laser Doppler anemometry have been used successfully to assess the velocity field, but they are rather impractical in fluidization because a fluidized bed is opaque and also because the probes sometimes have to withstand very harsh physicochemical conditions within the bed. They are also intrusive as probes may distort the flow in their vicinity. In recent years, sophisticated nonintrusive tomographic techniques are becoming available for the study of flow patterns in fluidization [2], but they carry significant costs and safety requirements. By contrast, pressure sensors are both robust and relatively cheap, can be readily used in industrial equipment, and in addition can be made virtually

nonintrusive. The main limitation of pressure is its intrinsically nonlocal nature due to the assumption of incompressibility of the flowing fluids. Nevertheless, pressure has been shown to be a useful quantity in turbulence research [3,4]. In the theory of multiphase flows, it is well established that local pressure fluctuations are representative of the hydrodynamics (e.g., Ref. [5,6]). Pressure at some point in the bed not only reflects local dynamics in the form of passing bubbles, but also the combined effect of bubble coalescence and breakup, bubble formation at the distributor plate and eruption at the surface, all taking place some distance away from the probe, therefore characterizing the dynamics of the bed as a whole [7]. Pressure data are typically used to validate fluidization regimes [8] and to measure bubble size [9]. Recently, analysis of local pressure measurements was used to advocate the chaotic behavior of fluidized beds [10–12] and to monitor the quality of fluidization [13].

II. STATISTICS OF PRESSURE FLUCTUATION MEASUREMENTS

This study uses pressure measurements performed at a sampling rate of 200 Hz at different positions inside a pilot-size fluidized bed, 80 cm in diameter, filled with sand particles of size 0.3–0.5 mm up to a settled bed height of 93 cm. Air was injected through a porous bottom plate, at superficial velocity U_0 ranging from 0.24 m/s to 0.70 m/s, corresponding to 1.7–5.0 times the minimum fluidization velocity. Kistler 7261 piezoelectric transducers, which measure the pressure relative to average ambient pressure with an accuracy of ≈ 10 Pa, were used for the measurement of pressure. The sensors, together with associated tubing, were tested for distortion of pressure fluctuation amplitude and phase. No significant influence of the dead volume was found at frequencies typical for gas-solid fluidized beds (0–50 Hz). During acquisition, data were low-pass filtered at 50 Hz.

The probability density function (PDF) of pressure fluctuations

$$\Delta P(t, \Delta t) = P(t + \Delta t) - P(t) \quad (1)$$

was evaluated for different time delays Δt , in a manner reminiscent of the analysis of longitudinal velocity

*Electronic address: S.Gheorghiu@tnw.tudelft.nl

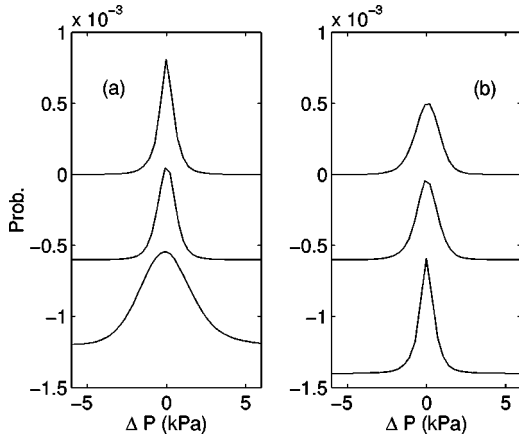


FIG. 1. PDF's of pressure fluctuations (1) $\Delta t = 10$ ms: (a) $U_0 = 1.7U_{mf}$, probe height $H = 0.84$ m, 0.54 m, 0.14 m (top to bottom); (b) probe height 0.84 m, gas velocity $U_0 = 5.0U_{mf}$, $2.8U_{mf}$, $1.7U_{mf}$ (top to bottom). The top row is to scale; the bottom two are shifted for clarity.

increments in a single-phase turbulence. While the use of PDF's in the characterization and monitoring of fluidized beds is not new (e.g., Ref. [14]), previous studies only addressed the PDF of the peak-to-peak pressure difference or the PDF of the pressure itself. In both cases, no temporal correlations between data points were taken into consideration. By contrast, our present calculation implicitly includes the time scale and dynamics of the variable, and is more robust since it removes artifacts due to fluctuations in the gas flow and any long-time trends in the data.

Figure 1 shows typical PDF's of pressure fluctuations (1), for time delay $\Delta t = 10$ ms, different gas velocities, and different probe heights. The PDF's are non-Gaussian, and a log-log representation reveals that the tails are represented by a power law, with large events much more frequent than expected in a normal distribution (Fig. 2). Very long-time series (roughly 1 h of 200-Hz data) were used to ensure accurate statistics.

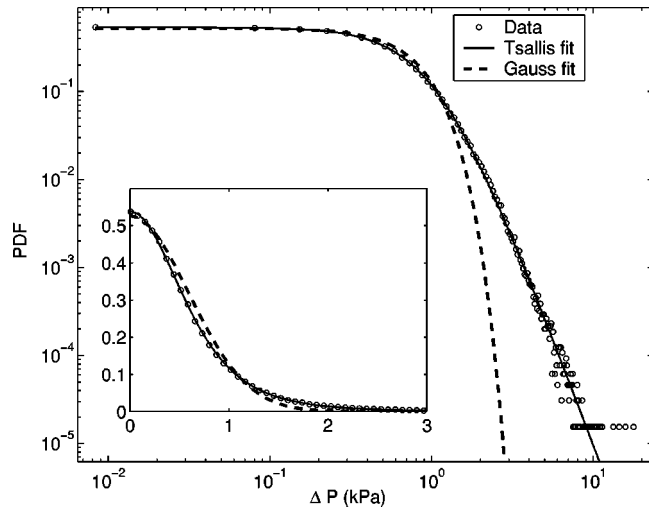


FIG. 2. Gaussian and Tsallis fits of the PDF for $U_0 = 1.7U_{mf}$, $H = 0.54$ m, $\Delta t = 10$ ms. Inset shows the fits in linear scale. Only the positive side of the PDF is shown for clarity.

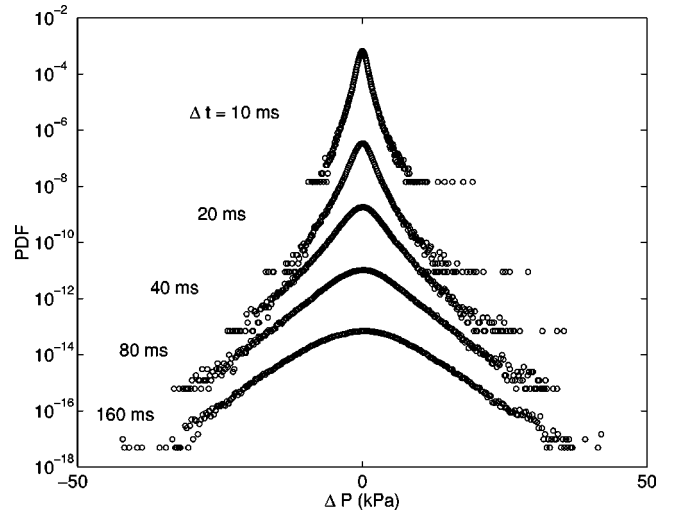


FIG. 3. Decay of the PDF to a Gaussian. $U_0 = 1.7U_{mf}$, $H = 0.54$ m. The top set is to scale, other sets are shifted down for clarity.

It has been known for several years that PDF's of velocity increments in a single-phase turbulence have the same qualitative features [15], a fact traditionally associated with intermittency. Recently, several researchers [16–18] proposed a novel explanation of this phenomenon based on nonextensive thermodynamics. Beck *et al.* showed that velocity increments in a high-precision measurement of Taylor-Couette flow can be fitted to a Tsallis PDF [19]:

$$\rho(u) = \frac{1}{Z_q} [1 + (q-1)\beta u^\alpha]^{1/(1-q)}, \quad (2)$$

where $\rho(u)$ denotes the probability density of the longitudinal velocity increments, β is related to the variance of u , while the so-called nonextensivity parameter q quantifies the departure from the Gaussian distribution, and α is a real parameter with a weak dependence on q . Z_q is seen as a q -dependent partition function that ensures normalization, and the “classic” expressions for ρ and Z of Boltzmann-Gibbs statistics are recovered if $q \rightarrow 1$.

Inspired by Beck's approach, we find that with considerable accuracy, PDF's of pressure fluctuations in fluidized beds are represented by

$$\rho(\Delta P) = \frac{1}{Z_q} [1 + (q-1)\beta|\Delta P|^\alpha]^{1/(1-q)}. \quad (3)$$

Numerical fits of the data using Eq. (3) give $\alpha = 2.0 \pm 0.05$, and a nonextensivity parameter q in the range 1.0–1.5 for $\Delta t = 10$ ms, for all probe heights and superficial gas velocities considered. All reported values refer to the positive side of the PDF. A typical dataset is shown in Fig. 2, with fitting parameters $q = 1.45$ (95% confidence interval [1.446, 1.455]) and $\beta = 1.33$ [1.328, 1.348]. With increasing time delay Δt , parameters q and β decrease: e.g., for measurements at $U_0 = 1.7U_{mf}$, $H = 0.54$ m, the values decay from $q = 1.45$, $\beta = 1.33$ at $\Delta t = 10$ ms, to $q \approx 1.0$, $\beta \approx 0.5$ at $\Delta t = 500$ ms. Therefore, the distribution is Gaussian for long-time delays (Fig. 3), a feature that has also been observed in turbulence

data. Considering the typical velocity of bubbles at given fluidization parameters, time scales up to 500 ms correspond roughly to spatial separations of the order of the largest bubbles in the bed (10–20 cm). There appear to be residual Tsallis statistics ($q \geq 1$) even at larger scales, but numerical fits corresponding to long-time delays are less consistent. To contrast the turbulence analysis, our numerical fits show a rather constant value $\alpha \approx 2.0$, as opposed to a q -dependent one, and also the variation of q is more significant.

The quality of the fit reveals another remarkable feature. Systematically, data for low superficial velocity ($U_0 = 1.7U_{mf}$) and a high probe position provide the best fits, and also the highest q values. As the gas flow is increased, the PDF still features well-defined fat tails, but only these tails are well represented by the theoretical distribution (3). Based on this observation, we conjecture that the signal has two components, only one of which satisfies Eq. (3). Indeed, in a fluidized bed there are at least two distinct contributions to the pressure. One is of local nature, represented by fluctuations caused by bubbles passing the probe. This disturbance travels at a relatively low velocity, accompanying each bubble as it rises. The other contribution is felt almost simultaneously throughout the entire bed, and is given by compression waves generated by the formation of bubbles at the bottom distributor plate, their coalescence, and their final burst at the top of the bed [7]. The fast propagation of the nonlocal compression waves allows, in principle, the separation of the two components by using two simultaneous pressure measurements at different positions in the bed.

The separation of the two components is typically done in frequency space [20]. For the purpose of analyzing PDF's, we devised an algorithm that uses the frequency information, but decomposes the signal in real space. Simultaneous pressure data $P(t)$ from a position within the bed and a position below the distributor plate [“windbox” pressure $P_w(t)$] were used. The distributor plate transmits any fast compression waves generated in the bed, but almost no bubble-induced fluctuations due to their localization property. The “bubble component” of P is then computed as $P_b(t) = P(t) - CP_w(t)$, where the constant C is chosen so that the coherent output power between P_b and P_w is minimal. If \hat{P}_w and \hat{P}_b denote the power spectral density of the windbox and bubble signals, and $\hat{X}_{b,w}$ denotes the cross spectral density of the two signals, then the coherent output power is defined as [20]

$$\mathcal{P}_{coh} = \gamma_{b,w} \hat{P}_w, \quad (4)$$

where $\gamma_{b,w} \in [0,1]$ is the coherence between the bubble and windbox signals,

$$\gamma_{b,w} = \frac{\|\hat{X}_{b,w}\|^2}{\hat{P}_b \hat{P}_w}. \quad (5)$$

In other words, the algorithm tries to remove all similarities to the windbox (bubbleless) signal from the measurement, leaving just the bubble component. Complete separation cannot be achieved due to distortion of the compression waves

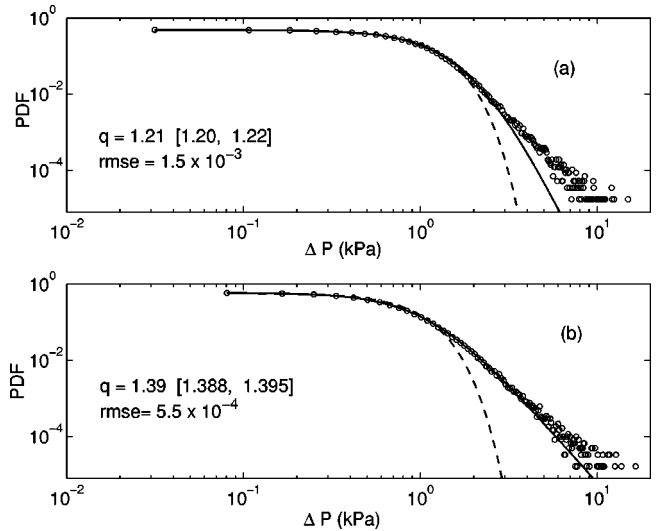


FIG. 4. Tsallis fits (solid lines) of the “raw” PDF (a) and bubble component PDF (b). $U_0 = 5.0U_{mf}$, $H = 0.84$ m, $\Delta t = 10$ ms. q values are accompanied by 95% confidence intervals and the root-mean-square error of the Tsallis fit. Gaussian fits (dotted) are shown for comparison.

by the porous distributor plate, the fact that upward and downward fast traveling waves have different attenuation factors, and also to the imperfect localization of the bubble pressure fluctuations.

The PDF of ΔP_b is analyzed in the same way as that of the original ΔP . The Tsallis fit (3) of the bubble component is better than the one corresponding to the raw data, as shown by an overall drop in the fitting error (Fig. 4). Additionally, the nonextensivity parameter q of the bubble component is significantly larger, indicating a more pronounced departure from a normal distribution. Meanwhile, the analysis of the windbox fluctuations ΔP_w yields a Gaussian fit of comparable quality (Fig. 5). The same value of parameter $\alpha \approx 2$ was found in both the raw data and the bubble component data.

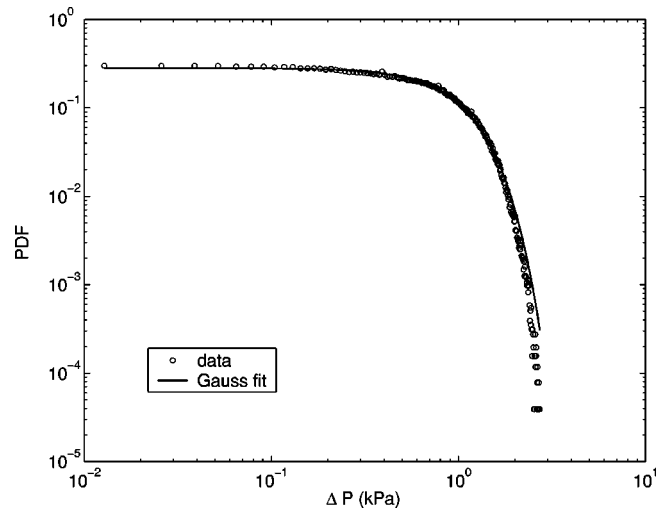


FIG. 5. Positive side of the PDF of the windbox signal and its Gaussian fit. $U_0 = 5.0U_{mf}$, $\Delta t = 10$ ms.

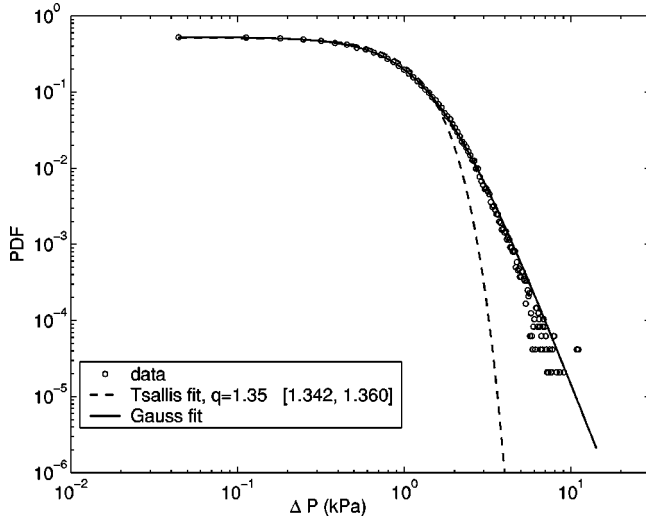


FIG. 6. Positive side of the PDF of ΔP_s , and corresponding Tsallis and Gauss fits. $U_0 = 5.0U_{mf}$, $H = 0.14$ m, $\Delta t = 10$ ms. The 95% confidence interval on q is shown.

To further consolidate the two-component picture, an alternative calculation was carried out using simultaneous pressure measurements P_1 and P_2 coming from two probes placed at the same height, but some horizontal distance away from each other. The two signals were subtracted, $P_s(t) = P_1(t) - P_2(t)$, and then the PDF of ΔP_s was computed as above. The fast-wave, coherent component of P_1 and P_2 is virtually the same and is therefore discarded, leaving a pure combination of “bubble signals.” The Tsallis fit of the PDF of ΔP_s is excellent (Fig. 6).

These results confirm the hypothesis that the bubble component of the pressure fluctuations is the sole carrier of the power-law characteristic. This conclusion is also supported by the previous observation that Tsallis fits are better for lower gas velocities U_0 and at higher positions in the bed. With increasing gas flow, the gas uptake of the column increases, together with the frequency of the phenomena that produce fast compression waves. Therefore, at higher gas flows, the bubble component of the signal is more distorted. Also, since bubbles produced at the bottom of the bed grow in size as they progress upwards, the bubble component is more pronounced at higher measurement positions.

III. MODELING AND THEORETICAL INTERPRETATION

Several researchers have proposed that the power-law form proposed by Tsallis for the probability of a microstate of energy ϵ ,

$$\rho(\epsilon) \sim [1 + (q-1)\beta\epsilon]^{1/(1-q)} \quad (6)$$

can arise from a weighted average over the Boltzmann factors of ordinary statistical mechanics ($e^{-\beta\epsilon}$), provided the weights are sampled from a gamma distribution [16,21,22]. If the temperature or, equivalently, the energy dissipation rate β fluctuates with the required distribution, even ordinary, conventional thermodynamic systems can display abnormal, nonextensivelike statistics. Similar observations on the

particle velocity distribution in granular systems [23–25] may apparently be explained using the same argument [47]. Here we propose that a similar mechanism is producing the Tsallis PDF of pressure fluctuations in a fluidized bed.

At any moment in time, a fluidized bed is a collection of bubbles of various sizes. The pressure disturbance associated with a passing bubble can be felt a certain distance away, so although no two bubbles coexist at the same position at the same time, a pressure sensor picks up a superposition of signals from bubbles in an area typically ~ 0.5 m around it [48].

The most widely used theoretical model for a bubble in a fluidized bed was given by Davidson and Harrison [26]. Derived from two-phase flow theory, it gives the pressure field around a passing spherical bubble with respect to the pressure at the observer’s location:

$$P(r, \theta) = \rho_s g (1 - \epsilon_{mf}) \begin{cases} \frac{R^3}{r^2} \cos \theta, & r \geq R \\ r \cos \theta, & r < R, \end{cases} \quad (7)$$

where r and θ are the polar coordinates of the observer with respect to the bubble center, R is the bubble radius, ρ_s is the density of the solid phase, and ϵ_{mf} is the void fraction corresponding to minimum fluidization. Furthermore, to a good approximation, the velocity of bubbles depends on their size as $u = 0.7\sqrt{2gR}$ [26].

We assume for simplicity that the pressure sensor is placed on the bubble path, the center of the bubble passes the observer at time $t = t_0$, and the bubble pierces the detector during the time interval $t_0 - T < t < t_0 + T$. We make the transformation $R = Tu$ and introduce new variables $P^* = P/[\rho_s g (1 - \epsilon_{mf})]$, and $t^* = 0.7t\sqrt{2g}$. This leads to

$$P^*(t^*) = \begin{cases} + \frac{R^2}{(t^* - t_0^*)^2}, & t^* < t_0^* - \sqrt{R} \\ - (t^* - t_0^*)\sqrt{R}, & |t^* - t_0^*| \leq \sqrt{R} \\ - \frac{R^2}{(t^* - t_0^*)^2}, & t^* > t_0^* + \sqrt{R}. \end{cases} \quad (8)$$

Figure 7 shows the pressure time-trace and its derivative.

A surrogate pressure signal consisting of bubbles of a fixed size R was constructed numerically as a superposition of pressure traces (8) of bubbles with randomly positioned centers t_0 . This is obviously not a complete model for the measured pressure signal since it lacks the fast-wave component, but it is a good representation of the “bubble component” that carries the power-law statistics, as discussed in the preceding section.

For short-time delays, $\Delta P^* \approx P^{*'} \Delta t^*$, and by differentiating Eq. (8) it is easy to see that the range of the variable ΔP^* is proportional to \sqrt{R} . Since the bubbles in this surrogate signal are identical and independent, the strong form of the central limit theorem guarantees that the PDF of the superposition is Gaussian,

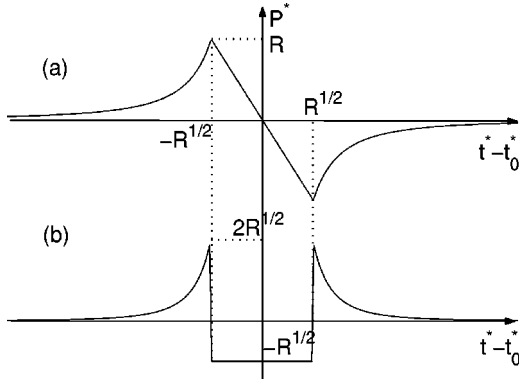


FIG. 7. Davidson-Harrison bubble, as seen by the sensor: pressure trace (a), derivative of the pressure (b).

$$\rho(\Delta P^*, R) = \frac{N}{\sqrt{R}} e^{-(c/R)\Delta P^{*2}}, \quad (9)$$

where N is the normalization factor and c depends on the number of bubbles that coexist at one moment in the bed. A similar, slightly more involved calculation allows the extension of this reasoning to bubbles traveling on paths that do not intersect the detector. Any random spatial distribution of identical bubbles can be shown to produce a normal distribution of pressure fluctuations (9), with a standard deviation proportional to \sqrt{R} .

Taking into account that in a freely bubbling bed, bubbles come in various sizes, an actual pressure measurement only samples the marginal probability distribution $\rho(\Delta P^*) = \int \rho(\Delta P^*, R) f(R) dR$, where $f(R)$ is the probability density function of bubble sizes in the fluidized bed. To assess the validity of the hypothesis that this weighted average is responsible for transforming the Gaussian PDF (9) of a one-size bubble signal into the Tsallis PDF (3) of the actual data, accurate statistics of bubble sizes are therefore needed.

A direct, accurate, real-time measurement of bubble size in a three-dimensional fluidized bed is very difficult to carry out. Tomographic techniques using x-rays, γ radiation, or electrical capacitance either do not have enough temporal resolution or have enough spatial resolution because of problems with the image reconstruction. Alternatively, simultaneous pressure measurements with multiple sensors can be used to assess bubble size in multiphase flows [9,27]. Although leading to more reliable data, these methods are still ill-conditioned in the language of inverse problems, and typically need some *a priori* assumption about the bubble shape and size distribution. Due to these difficulties and the lack of a solid theoretical basis for understanding the process of bubble creation and growth in fluidized beds, measured bubble size data have so far been empirically fitted to a γ [28–31], Rayleigh [29,30], or log-normal distribution function [32].

Here we propose an expression for the bubble size distribution in the form

$$f(R) = CR^{-\tau} e^{-a/R}, \quad (10)$$

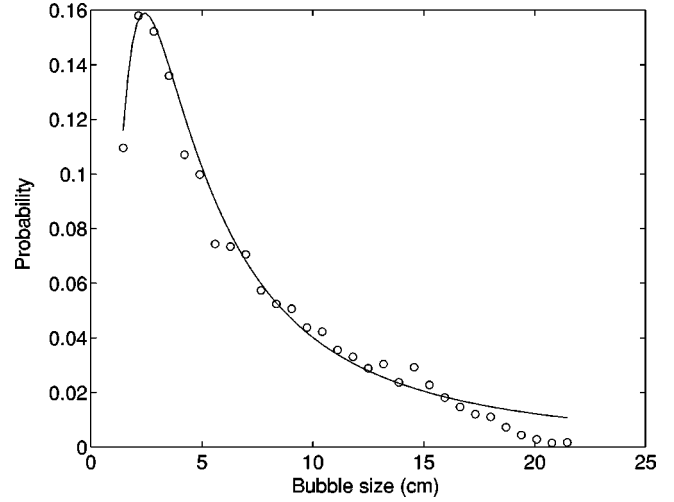


FIG. 8. Distribution of bubble sizes near the top of a 40 cm, two-dimensional fluidized bed from video data. $U_0 = 3.0U_{mf}$. The solid line is the fit to Eq. (10).

with real parameters $a, \tau > 0$, and normalization constant C . This conjecture is based on the assumption that bubbles grow as they progress upwards by coalescence of smaller bubbles, in a process of aggregation described by a Smoluchowski-type equation (e.g., Refs. [33–35]). The place of time in the classical treatment of aggregation is taken here by the vertical measurement position. Under fairly general conditions on the “coagulation kernel” [36,37], Eq. (10) would be an accurate representation of the skewed, bell-shaped distribution for moderate bubble sizes, high enough in the bed for coalescence to be fully developed. The power-law decay has an exponential cutoff at small R due to the fact that although only small bubbles are injected at the bottom of the bed, they progressively disappear by merging to form bigger bubbles higher up in the bed. The proposed distribution (10) was fitted on bubble size data extracted from video recordings of a two-dimensional bed with satisfactory results (Fig. 8).

Observing that Eq. (10) is a gamma distribution in variable $1/R$, we obtain for the PDF of pressure fluctuations

$$\begin{aligned} \rho(\Delta P^*) &\sim \int_0^\infty \frac{1}{\sqrt{R}} e^{-(c/R)\Delta P^{*2}} R^{-\tau} e^{-a/R} dR \\ &= \int_0^\infty e^{-(a+c\Delta P^{*2})/R} \left(\frac{1}{R}\right)^{\tau-3/2} d\left(\frac{1}{R}\right) \\ &= \Gamma\left(\tau - \frac{1}{2}\right) a^{(1/2)-\tau} \left(1 + \frac{c}{a}\Delta P^{*2}\right)^{(1/2)-\tau}, \quad (11) \end{aligned}$$

as long as $\tau > 3/2$. This expression is precisely of the form (3), with $\alpha = 2$,

$$q = 1 + \frac{1}{\tau - 1/2}, \quad (12)$$

and $c/a = \beta(q-1)[\rho_s g(1 - \epsilon_{mf})]^2$. Parameter q is related through τ to the details of the bubble growth mechanism.

To accurately capture the full bubble size distribution, Eq. (10) must be amended by an exponential decay at large R , since in agglomeration phenomena the cluster size distribution typically drops faster than any power law at large R [35–37]. Also at large R , bubble breakup combined with finite-size effects become significant, so that bubbles cannot grow without limit. Consequently, the PDF of pressure fluctuations in fluidized beds will typically fall slightly *below* the theoretical PDF of Eq. (11) in the range of very large ΔP . The departure of the bubble size distribution from the “ideal” form (10) may be slow to set in, especially in large systems, so the departure of the PDF from Eqs. (3) and (11) may not be actually visible in measured data.

IV. RELEVANCE TO “NONEXTENSIVE THERMOSTATISTICS”

In recent years, we are witnessing an increasing interest in the formalism and applications of nonextensive statistical mechanics, first proposed by Tsallis [38] and since developed by many others. The creators of this field argue that a generalized version of classical statistical mechanics may be more appropriate to describe the physics of systems operating far from equilibrium, many-body systems with long-range interactions [39,40], systems displaying anomalous diffusion [41–43], or operating at the edge of chaos [44,45]. Central to the theory is the postulate that a power-law form as given by Eq. (6) should replace the classic exponential Boltzmann factor $e^{-\beta\epsilon}$. The conceptual framework of statistical mechanics is preserved if the expression for entropy is also altered,

$$S_q = \frac{1}{q-1} \left(1 - \sum_i \rho_i^q \right), \quad (13)$$

where ρ_i is the probability of a microstate i of the system. Indeed, the Tsallis probability distribution maximizes the Tsallis entropy (13), just like the Boltzmann-Gibbs probability maximizes the Shannon-Gibbs entropy in classical statistical mechanics. The striking feature of the new entropy is its nonextensivity. If A and B are two independent systems, then

$$S_q(A+B) = S_q(A) + S_q(B) + (1-q)S_q(A)S_q(B). \quad (14)$$

All features of the ordinary, extensive thermostatics are recovered in the limit $q \rightarrow 1$.

It is important to point out that although the relevant variables in the present study fit remarkably well in the context of Tsallis statistics, and although the PDF of pressure maximizes its associated Tsallis entropy, there is no reason to expect fluidized beds to be nonextensive in the strict sense or anomalous in any other way. The observed statistics were explained under the explicit assumption that there are *no* spatial or temporal correlations between individual bubbles in the fluidized bed, as required by the central limit theorem. This assumption is accurate in the bubbling regime of fluidization, for large enough beds, and away from reactor walls so as to limit correlations induced by finite-size effects. Passing bubbles sometimes create local paths of low voidage that influence the movement of nearby bubbles, thus inducing

some space-time correlations. Fluidized beds are also known to have episodes of (pseudo)periodicity, but all these effects are minimal and do not characterize the hydrodynamics. It is therefore appropriate to consider that bubbles follow each other in a stochastic manner, a conclusion that is supported by various statistical tests on the distribution of interbubble time intervals [49].

The Tsallis form of the distribution of pressure fluctuations arises purely through the polydispersity of the bubble population. The assumed distribution of bubble sizes is the result of an agglomeration process, in which individual bubbles grow by coalescence of smaller ones. Judging by the ubiquity of aggregation phenomena in the physical world, spanning from aerosol science to polymers, astrophysics, and even to the dynamics of human populations, the mechanism outlined here may be a very prolific way of producing the Tsallis distributions in systems that are neither far from equilibrium nor possess long-range interactions, nor are subject to anomalous diffusion. This intriguing fact and the growing number of experimental observations [50] of the Tsallis statistics call for a careful review of the principles, applicability range, and nomenclature of nonextensive thermodynamics [46].

V. CONCLUDING REMARKS

We have shown that pressure fluctuations in bubbling fluidized beds are very well fitted by a probability density function with power-law tails, typically used in the context of the Tsallis statistics. Although these experimental observations are reminiscent of intermittency in fully developed single-phase turbulence, we must point out that turbulence is *not* a likely explanation for the observed behavior of fluidized beds. In the bubbling regime, the gas-particle mixture is much too dense and viscous for multiphase turbulence to develop (it most certainly plays a role at much higher gas flow rates). Also, the magnitude of pressure fluctuations analyzed here (typically up to 20 kPa) rules out the possibility that they are produced by air turbulence within individual bubbles.

The proposed representation is particularly accurate in large-size fluidized beds, which make it readily applicable to industrial equipment. By separating the different contributions to the pressure signal, it was shown that the remarkable statistics are contained in the localized pressure signal of the sequence of bubbles passing close to the detector. The shape of the PDF is explained through the folding of a Gaussian distribution (corresponding to a set of bubbles of the same size) onto a gamma distribution of variable $1/R$, where R is the bubble radius. The proposed bubble size distribution is seen as the result of an agglomeration process.

Fluidized beds appear as a prototype of a larger class of systems which may display Tsallis-like statistics in the relevant variables, without being intrinsically nonextensive. Interestingly, the fact that the Tsallis expression of entropy is the analog of the Shannon-Gibbs entropy for systems with a Tsallis PDF makes its formalism useful for the information-theoretic description (characterization, validation) and monitoring of multiphase flow regimes, understanding, nevertheless, that the observed phenomena share no fundamental relationship with nonextensive thermodynamics.

ACKNOWLEDGMENTS

We thank F. Kleijn van Willigen for the analysis of the two-dimensional bed video footage, and C. Tsallis, A. Robledo, T. Odijk, and S. Luding for illuminating discussions.

S.G. acknowledges support from the Delft University of Technology and M.-O.C. is grateful for the support of the Dutch National Foundation for Scientific Research (NWO) by way of a PIONIER grant and Open Competition Grant No. 98035.

-
- [1] D. Kunii and O. Levenspiel, *Fluidization Engineering*, 2nd ed. (Butterworth-Heinemann, Boston, 1991).
- [2] M.P. Dudukovic, *Exp. Therm. Fluid Sci.* **26**, 747 (2002).
- [3] M. Nelkin and S. Chen, *Phys. Fluids* **10**, 2119 (1998).
- [4] R.J. Hill and J.M. Wilczak, *J. Fluid Mech.* **296**, 247 (1995).
- [5] J.F. Davidson, *AIChE Symp. Ser.* **87**, 1 (1991).
- [6] J.G. Yates and S.J.R. Simmons, *Int. J. Multiphase Flow* **20**, 297 (1994).
- [7] J. van der Schaaf, J.C. Schouten, and C.M. van den Bleek, *Powder Technol.* **95**, 220 (1998).
- [8] F. Johnsson, R.C. Zijerveld, J.C. Schouten, C.M. van den Bleek, and B. Leckner, *Int. J. Multiphase Flow* **26**, 663 (2000).
- [9] N.N. Clark and C.M. Atkinson, *Chem. Eng. Sci.* **43**, 1547 (1988).
- [10] M.L.M. van der Stappen, J.C. Schouten, and C.M. van den Bleek, *AIChE Symp. Ser.* **296**, 91 (1993).
- [11] J.C. Schouten and C.M. van den Bleek, *AIChE Symp. Ser.* **88**, 70 (1992).
- [12] C.M. van den Bleek, M.-O. Coppens, and J.C. Schouten, *Chem. Eng. Sci.* **57**, 4763 (2002).
- [13] J.R. van Ommen, M.-O. Coppens, C.M. van den Bleek, and J.C. Schouten, *AIChEJ.* **46**, 2183 (2000).
- [14] S.C. Saxena, N.S. Rao, and V.N. Tanjore, *Exp. Therm. Fluid Sci.* **6**, 56 (1993).
- [15] A. Noullez, G. Wallace, W. Lempert, R.B. Miles, and U. Frisch, *J. Fluid Mech.* **339**, 287 (1997).
- [16] C. Beck, *Phys. Rev. Lett.* **87**, 180601 (2001).
- [17] T. Arimitsu and N. Arimitsu, *Phys. Rev. E* **61**, 3237 (2000).
- [18] F.N. Ramos, C.R. Neto, and R.R. Rosa, e-print cond-mat/0010435.
- [19] C. Beck, G.S. Lewis, and H.L. Swinney, *Phys. Rev. E* **63**, 035303(R) (2001).
- [20] J. van der Schaaf, J.C. Schouten, F. Johnsson, and C.M. van den Bleek, *Int. J. Multiphase Flow* **28**, 865 (2002).
- [21] G. Wilk and Z. Wlodarczyk, e-print hep-ph/0004250.
- [22] G. Wilk and Z. Wlodarczyk, *Phys. Rev. Lett.* **84**, 2770 (2000).
- [23] Y.-H. Taguchi and H. Takayasu, *Europhys. Lett.* **30**, 499 (1995).
- [24] Y. Murayama and M. Sano, *J. Phys. Soc. Jpn.* **67**, 1826 (1998).
- [25] R. Cafiero, S. Luding, and H.J. Herrmann, *Phys. Rev. Lett.* **84**, 6014 (2000).
- [26] J.F. Davidson and D. Harrison, *Fluidized Particles* (Cambridge University Press, Cambridge, 1963).
- [27] J.M. Burgess, A.G. Fane, and C.J.D. Fell, *IEEE Trans. Ind. Electron.* **60**, 249 (1982).
- [28] K.S. Lim and P.K. Agarwal, *Powder Technol.* **63**, 205 (1990).
- [29] N.N. Clark, W. Liu, and R. Turton, *Powder Technol.* **88**, 179 (1996).
- [30] W. Liu and N.N. Clark, *Int. J. Multiphase Flow* **21**, 1073 (1995).
- [31] P. Selegheim and F.E. Milioli, *Powder Technol.* **115**, 114 (2001).
- [32] T. Chiba, K. Terashima, and H. Kobayashi, *J. Chem. Eng. Jpn.* **8**, 167 (1975).
- [33] S. Chandrasekhar, *Rev. Mod. Phys.* **15**, 1 (1943).
- [34] R.M. Ziff, E.M. Hendricks, and M.H. Ernst, *Phys. Rev. Lett.* **49**, 593 (1982).
- [35] T. Vicsek and F. Family, *Phys. Rev. Lett.* **52**, 1669 (1984).
- [36] M.H. Ernst, *Fundamental Problems in Statistical Mechanics VI*, edited by E.G.D. Cohen (North-Holland, Amsterdam, 1985).
- [37] P.G.J. van Dongen and M.H. Ernst, *Phys. Rev. Lett.* **54**, 1396 (1985).
- [38] C. Tsallis, *J. Stat. Phys.* **52**, 479 (1988).
- [39] V. Latora, A. Rapisarda, and C. Tsallis, *Physica A* **305**, 129 (2002).
- [40] V. Latora, A. Rapisarda, and C. Tsallis, *Phys. Rev. E* **64**, 056134 (2001).
- [41] C. Tsallis, S.V.F. Levy, A.M.C. Souza, and R. Maynard, *Phys. Rev. Lett.* **75**, 3589 (1995).
- [42] L. Borland, *Phys. Rev. E* **57**, 6634 (1998).
- [43] D.H. Zanette and P.A. Alemany, *Phys. Rev. Lett.* **75**, 366 (1995).
- [44] F. Baldovin and A. Robledo, e-print cond-mat/0205356; e-print cond-mat/0205371.
- [45] M.L. Lyra and C. Tsallis, *Phys. Rev. Lett.* **80**, 53 (1998).
- [46] A. Cho, *Science* **297**, 1268 (2002).
- [47] S. Luding (private communication).
- [48] J.R. van Ommen (unpublished).
- [49] S. Baltussen, Z. Kolar, C.M. van den Bleek, and M.-O. Coppens (unpublished).
- [50] See <http://tsallis.cat.cbpf.br/biblio.htm>.